TISSUE ENGINEERING: Part A
Volume 19, Numbers 15 and 16, 2013

DOI: 10.1089/ten.tea.2012.0421

Voluntary Movement Controlled by the Surface EMG Signal for Tissue-Engineered Skeletal Muscle on a Gripping Tool

Ken-ichiro Kabumoto, ME,[1] Takayuki Hoshino, PhD,[2] Yoshitake Akiyama, PhD,[2] and Keisuke Morishima, PhD[2]

We have developed a living prosthesis consisting of a living muscle-powered device, which is controlled by neuronal signals to recover some of the functions of a lost extremity. A tissue-engineered skeletal muscle was fabricated with two anchorage points from a primary rat myoblast cultured in a collagen Matrigel mixed gel. Differentiation to the skeletal muscle was confirmed in the tissue-engineered skeletal muscle, and the contraction force increased with increasing frequency of electric stimulation. Then, the tissue-engineered skeletal muscle was assembled into a gripper-type microhand. The tissue-engineered skeletal muscle of the microhand was stimulated electrically, which was then followed by the voluntary movement of the subject's hand. The signal of the surface electromyogram from a subject was processed to mimic the firing spikes of a neuromuscular junction to control the contraction of the tissue-engineered skeletal muscle. The tele-operation of the microhand was demonstrated by optical microscope observations.

Introduction

Amputations as a result of accidents and diseases decrease the quality of life (QOL) for patients who experience them. Prosthetic devices are needed by individuals who are disabled, particularly those who have lost limbs, sustained myopathies, or suffer from diseases of the nervous system. The treatments offered for amputees have mainly consisted of providing prosthetic devices to restore some degree of the functions that would have been provided for their life.[1–5] It has been desired that prosthetic technologies have an equivalent performance to be a native neuromuscular control system. Motorized prosthetic limbs have a potential to contribute to an increased QOL by supporting dynamic motion of their users.[1–5] A motorized prosthetic arm is one of the motion-supporting systems for amputees that reconstructs the motor function, including the somatic and tactile sensation using a direct connection to the nervous system.[4,6] A directly connected neural prosthesis can provide a high degree of voluntary arm movements on the robotic arm making it seem like the lost natural arm.[1]

Moreover, an engineered muscle tissue to replace the motor device in the prosthetic arm can be expected to reach the performance of a natural arm, since the signaling can be easily connected to the nervous system, the tissue has biocompatibility for an implantable device, and the tissue also has a sustainable power supply from the recipient metabolism. Therefore, we propose a living prosthesis consisting of a living skeletal muscle based on tissue-engineering techniques. The concept of the living prosthesis will allow a patient to recover the motor control on the living muscle and neural signals, and this indicates that the living prosthesis can be driven mainly by the metabolic energy in the human body.

The tissue-engineered muscle was previously reported to restore lost neuromuscular connections for treatment of traumatic injuries, congenital defects, tumor ablation, prolonged denervation, a variety of myopathies (such as Duchene muscular dystrophy), and spinal muscular atrophy. A cultured mixture with myoblasts[7–19] or cardiomyocytes[20,21] and hydrogel with collagen and Martigels was successfully used to reconstruct the contracting function in a molded shape.[22,23] Also, alignment and differentiation to contractile muscle tissues were reported as a culture on a grooved microstructure made of poly(dimethyl siloxane) (PDMS)[24] and methacrylated gelatin.[25] The tissue-engineered skeletal muscles have been previously researched regarding cellular alignment and contractile activities to mimic the natural skeletal muscle[24,25] and to connect neurons to the tissue-engineered skeletal muscle[26] for improvement of the contractile function. These aligned and neural connected engineered skeletal muscles should be controlled the contractile function to be followed human voluntary command via direct connection of neuromuscular junctions or via neuronal signals of human interface. Thus, we focused on the reconstruction of a muscle tissue *in vitro* to replace an artificial equipment as a living component in the prosthesis. We

[1]Department of Bio-Application and Systems Engineering, Tokyo University of Agriculture and Technology, Tokyo, Japan.
[2]Department of Mechanical Engineering, Osaka University, Osaka, Japan.

report a tissue-engineered skeletal muscle that was designed as an alternative actuator to a conventional electric motor in a step toward the next generation of prostheses.

We investigated the reconstruction of the muscle tissue with a high hierarchal structure, which included the cell alignment along the higher order structure to get contraction behavior similar to that of a native muscle and used a snap-in anchor for assembly into the mechanical part of the prosthesis. Finally, we also demonstrated a muscle-powered gripper-type microhand *in vitro*, which was controlled using the electromyogram (EMG) signals from the forearm of a human subject.

Materials and Methods

Control system using surface EMG for muscle-powered microhand

Our teleoperation system of a gripper-type microhand (Fig. 1) was combined surface EMG for master control and a tissue-engineered slave actuator. Operators could teleoperate the muscle-powered microhand by using forearm surface EMG. Since the surface EMG signal resulted from firing active potentials of neuromuscular units of the contracting muscle, we mimicked the neuromuscular junction of the operator's forearm muscle using an inverse signal processing from the surface EMG. The neuromimetic spike signal from the surface EMG was connected to the tissue-engineered skeletal muscle of the microhand via an electrical stimulator (Nihon kohden). The microhand was placed on an inversed microscope (Ti-S; Nikon) with a CCD camera (30 frame/s) to observe the displacement of the microhand due to contraction of the tissue-engineered skeletal muscle.

Preparation of primary skeletal myoblasts

Primary skeletal myoblasts were isolated from 1-day-old Wister rats as previously described.[17] All skeletal muscle tissues were dissected from the hind limbs and dissociated by the mincing solution containing 50 U/mL collagenase type IV (Gibco Invitrogen Co.) and 4 U/mL dispase (Gibco Invitrogen Co.). The slurry was suspended in the growth medium consisting of Ham's F-12 (Gibco Invitrogen Co.), 20% fetal bovine serum (Gibco Invitrogen Co.), 100 U/mL penicillin, and 100 μg/mL streptomycin.

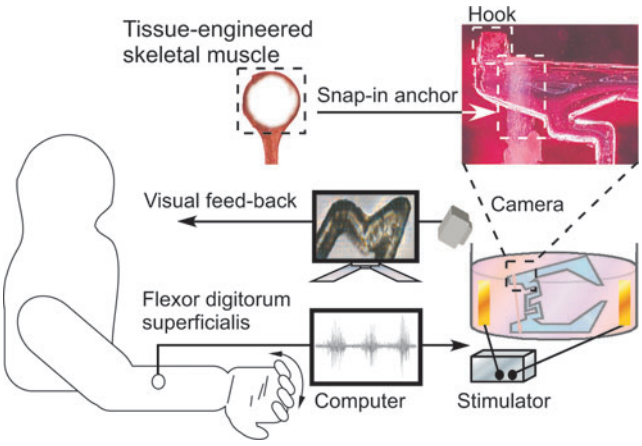

FIG. 1. Schematic of control system using electromyogram (EMG) signals for muscle-powered hand. The microhand with attached skeletal muscle tissue was activated by human EMG signals and feedback by motion capture analysis. Color images available online at www.liebertpub.com/tea

Fabrication of engineered skeletal muscle tissue

The tissue-engineered skeletal muscle tissue was fabricated by mixing primary rat skeletal myoblasts with bioactive hydrogel and culturing in cellular media.[27] The skeletal myoblast/gel suspension was obtained by mixing isolated skeletal myoblasts (1.0×10^7 cell/mL), collagen I (Rat Tail Collagen, Type I, BD Bioscience), and a basement membrane protein mixture (Matrigel; BD Bioscience). The suspension was gelated, cast into hydrophilically augmented PDMS molds, and incubated for 3 h at 37°C and 5% CO_2. Finally, the suspension was placed in the growth medium. After culture day 3, the growth medium in the tissue-engineered skeletal muscles was switched to the differentiation medium consisting of the high-glucose Dulbecco's Modified Eagle's Medium (Gibco Invitrogen Co.), 10% horse serum (Gibco Invitrogen Co.), and 100 U/mL penicillin and 100 μg/mL streptomycin. These protocols were partially modified based on Ref.[11,27]

Design of engineered skeletal muscle tissue

The tissue-engineered skeletal muscle was designed to be an actuator of the microhand, which mimicked a finger in micro. The direction of the tissue-engineered skeletal muscle contraction had to be determined as unidirectional muscle tissues. The end of the tissue-engineered skeletal muscle was looped to allow it to be snapped to the hook of the microhand. Thus, the PDMS molds of tissue-engineered skeletal muscles were designed with a beam shape and two loops, one on each end. The loops were molded by two pillars, which were placed in the ends of the molds to anchor the beam-shaped gel. The tissue-engineered skeletal muscle was designed to have an hierarchal structure, including highly aligned myotubes differentiated unidirectionally, and the snap-in connector to be assembled in the prosthesis. The high alignment of the myotubes to the gel structure was obtained by unidirectionally aligning myoblasts along the geometric structure[14,16,18,19,28] and using the inner stress[27] of the gel structure.

Electrophysiological analysis

Electrical responsiveness of the tissue-engineered skeletal muscle was analyzed during electrical pulse stimulation (EPS). Electrical pulses generated by an electrical stimulator (SE-3301; Nihon kohden) were applied to the skeletal muscles in the medium through two electrodes. To reduce electrolysis, a 220 μF aluminum electrolytic capacitor was connected between the stimulator and the anode electrode in the cell culture dish.[29] The stimulating voltage and the pulse duration were 50 V and 40 ms, respectively. An LED light flash was synchronized to the electrical stimulation pulses, which indicated the onset trigger on the video images. The tissue-engineered skeletal muscles were observed with an inverted optical microscope (IX-71; Olympus) during electrical stimulation and the video images were recorded onto a computer. Displacements of the contraction were tracked using commercial software for motion analysis (DippMotionPro2D; DITECT Co.).

Quantitative analysis of cellular alignment

The cell alignment angle was quantified from optical microscopic images using image processing software (ImageJ NIH). The cell images in the tissue-engineered skeletal muscle and on a cell culture dish were acquired on culture day 12. Acquired images were captured as 640×480 pixels with an 8-bit grayscale resolution. Briefly, the following procedure was used.

1) Edges in the image were highlighted by applying a Difference of Gaussians (DOG) operation.
2) The DOG images were converted to binary images and then, dilating and eroding (morphological operations) were carried out to close the holes between the objects.
3) The binary images were separated in the nonoverlapping 20×20 pixels subregions. The alignment was evaluated using distribution of local cellular alignment angles in subregions of five samples and deviations of the local angles. The orientation of each subregion was calculated using ImageJ Plug-in.[30] Briefly, each orientation of each subregion was calculated as a local mean angle based on the partial spatial derivatives of the subregion image along the principal directions. Error bars represent standard deviation, with $n=5$ for viability studies. Statistical significance was determined using the Student's t-test.

Histological staining

The cell alignment and cell morphology inside of a tissue-engineered skeletal muscle was assessed by histological staining. The tissue-engineered skeletal muscles on culture day 14 were sliced and stained with hematoxylin and eosin (HE) after being fixed with PBS containing 4% paraformaldehyde.

Immunostaining

To check for immunofluorescence, following the method of Fujita *et al.*,[31] tissue-engineered skeletal muscles on culture day 29, were fixed with PBS containing 4% paraformaldehyde for 15 min, permeabilized with 0.2% Triton-X for 15 min, and then blocked with 1% bovine serum albumin for 30 min. After the blocking, the tissue-engineered skeletal muscles were treated with the monoclonal anti-α-actinin antibody (A-7811; Sigma Aldrich) for 60 min and the goat anti-mouse IgG antibody-conjugated Alexa 488 (A-11001; Invitrogen) for 45 min. A confocal microscope system (TE-2000, Nikon; CSU-X1, Yokogawa) was used to take muscle sample images with a cooled CCD camera (iXon^{EM+}; Andor). The confocal images were processed by deconvolution and stacked at the maximum intensity to evaluate differentiation to the myotubes and their alignment.

Design and fabrication of the microhand

The microhand was designed to be a gripping device powered by the tissue-engineered muscle. As shown in Figure 1, the tissue-engineered skeletal muscle was assembled on the end of the PDMS microhand. The tip of the microhand was opened by the muscle contraction. The microhand was fabricated by a typical microfabrication technique, which consisted of molding PDMS (Silpot 194; Dow corning) prepolymer with a 10% curing agent on a photolithographic SU-8 (SU-8 3050; Microcham) mold followed by curing at 80°C for 1 h.

Measurement of contraction force of tissue-engineered skeletal muscle

The contraction force was measured using bending of the microhand powered by the tissue-engineered skeletal muscle. To determine the frequency response to stimulation, 1–10 Hz electrical stimulations were applied to the tissue-engineered skeletal muscle assembled with the PDMS microhand. The stimulating voltage and the pulse duration were 50 V and 40 ms. The displacement of the tip of the microhand was recorded using a video camera on an inverted microscope (Ti-S; Nikon) during the electrical stimulations. The displacement of the microhand was determined using image analysis software (DippMotionPro2D; DITECT Co.). The dynamic force response to the electrical stimulation was calculated from the displacement of the microhand.

Generating muscle control signal from surface EMG

The muscle control signal of the gripper-type microhand was processed from surface EMG of the human subject (Fig. 1) on the LabVIEW (National Instruments) program. The generated function of the muscle control was on a neuromimetic firing spike signal of muscle contraction. There are four steps in the signal processing to convert the surface EMG to a neuromimetic firing spike signal.

1) The surface EMG signal was rectified and integrated to be an integrated EMG with 100 ms of sliding time-window. An integrated EMG signal (V_{iEMG}) was given by

$$V_{iEMG}(t) = \int_0^{T_i} |V_{sEMG}(t+\tau)| d\tau \tag{1}$$

where V_{sEMG} and t are surface EMG and an arbitrary time value, respectively. The integration period T_i was 100 ms for EMG processing.

2) Amplitude of the integrated EMG signal was modulated by frequency using a sine function. The frequency-modulated integrated EMG signal (f_{iEMG}) was expressed as follows

$$f_{iEMG} = \sin(V_{iEMG}). \tag{2}$$

3) A high-pass filter was applied to cut off lower frequency of V_{iEMG}. The filtered signal (V_{hpf}) was shown using a filter function [$HPF(x)$] as

$$V_{hpf} = HPF(f_{iEMG}). \tag{3}$$

4) The neuromimetic firing spike signal was processed using the threshold of V_{hpf}. The tissue-engineered skeletal muscle was stimulated electrically by the following pulsed signal (V_{ens}).

$$V_{ens} = \begin{cases} 1, & V_{hpf} \geq k \\ 0, & V_{hpf} \leq k \end{cases} \tag{4}$$

where k is the threshold value.

Neuromimetic control for tissue-engineered skeletal muscle with microhand

The surface EMG signal was measured for the flexor digitorum superficialis muscle of the forearm. A reference electrode was attached on the ipsilateral elbow. Surface EMG was measured at 1 kHz and deformation of the microhand was recorded at about 30 Hz with the CCD camera (30 fps) set on the microscope (Ti-S; Nikon). The images were analyzed using motion analysis software.

Whenever V_{ens} was over the threshold k, the contraction of the tissue-engineered skeletal muscle was induced by electrical pulse stimuli at 50 V amplitude and 40 ms pulse width in the culture medium. The pulse onset trigger was controlled by the mimetic neuronal firing signal.

Results and Discussion

Formation of tissue-engineered skeletal muscle

Figure 2A shows the cell–gel mixture, which was placed into the PDMS molds. The shrinking cell–gel mixture became beam-shaped skeletal muscle tissues after culturing for 5 days. After around 19 days, the tissue-engineered skeletal muscles often contracted spontaneously; this confirmed that they had obtained contractile ability. Finally, the tissue-engineered skeletal muscles retained their beam shape after culturing for 45 days.

The contractile response of the tissue-engineered skeletal muscle to electrical pulse stimuli after culture day 21 was evaluated by image analysis. Contraction by stimulations at 1 Hz is shown in Figure 2B. The tissue-engineered skeletal muscle contracted according to the stimulations.

Morphological analysis of tissue-engineered skeletal muscles

Figure 3 shows the tissue-engineered skeletal muscle after culture day 14, stained with HE. The cell density near the surface was clearly higher than around the center (Fig. 3B). This result could be explained by hypothesizing that the cells necrotize around the center of the tissue-engineered skeletal muscle due to oxygen and nutrient deficiencies.[8] α-Actinin expressed on myotubes in the tissue-engineered skeletal muscle was labeled at culture day 39. Fluorescence imaging of α-actinin was done after fixation. The differentiation of myoblasts to myotubes was confirmed by the immunofluorescence imaging. Figure 3C indicates the myotubes aligned to the longitudinal axis on the gel surface of the tissue-engineered skeletal muscle.

HE staining and confocal imaging of α-actinin in the tissue-engineered muscle indicated that the skeletal muscle cells were aligned to the longitudinal direction on the tissue surface. In this research, we focused on the control method and the mechanical interface of the unidirectional aligned tissue-engineered skeletal muscle for a mechanical prosthetic application. Therefore, we stained alpha-actinin to evaluate the ratio of the contractile muscle cells in the tissue. Generally, alpha-actinin localizes to the Z-disc of myotubes, where they help anchor the myofibrillar actin filaments. Alpha-actinin immune staining could imply a formation of myotubes. Alpha-actinin-labeled myotubes aligned in longitudinal axis of the engineered tissue. And Figure 3A and 3B clearly showed formation of multiple nuclei in longitudinal myotubes along the tissue surface. These results suggested that some myotubes were formed on only the surface layer of the engineered tissues, although mechanical contraction forces were enough strong to drive the microgripper. To fabricate full packing muscles in engineered tissues, it

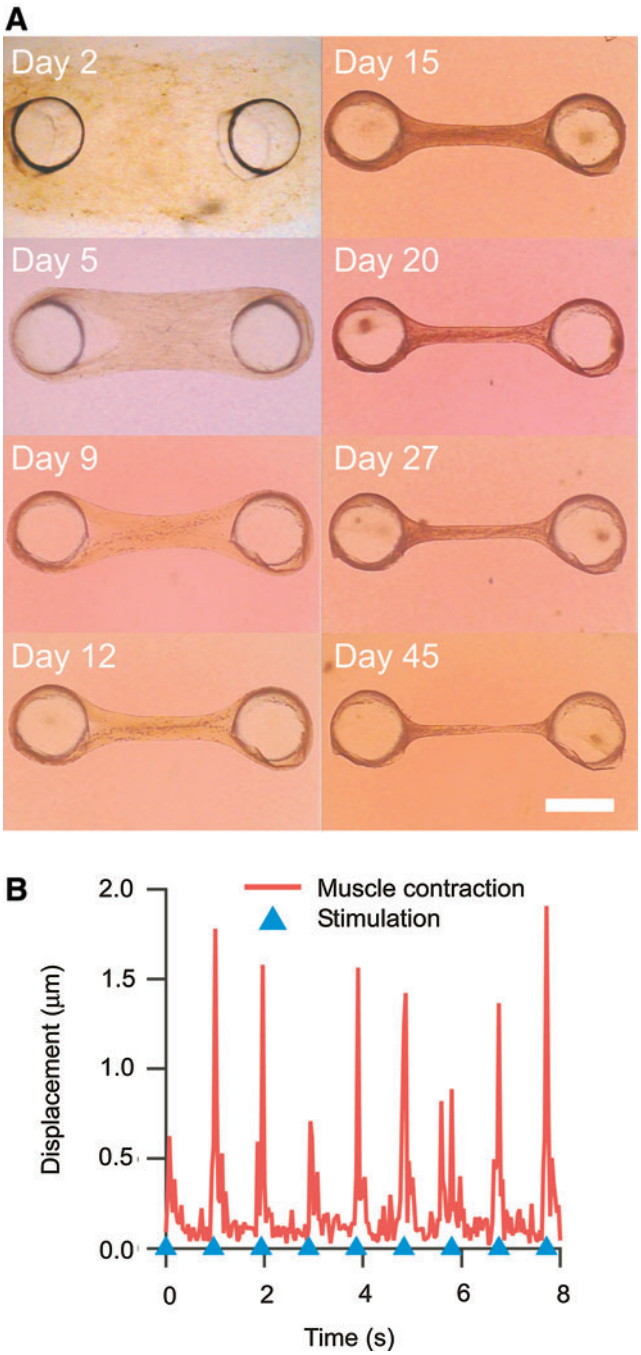

FIG. 2. Shrinkage of the tissue-engineered skeletal muscle during culturing. **(A)** Serial images of the tissue-engineered skeletal muscle. After culture day 2, the tissue-engineered skeletal muscle started to agglutinate around the anchor. Tissue-engineered skeletal muscles kept the beam shape after culturing for 45 days. **(B)** Example of muscle contraction evoked by electrical pulse stimulation (EPS). Response of the tissue-engineered skeletal muscle to EPS at frequency of 1 Hz. The blue triangles show the onset of EPS. The scale bar shows 1 mm. Color images available online at www.liebertpub.com/tea

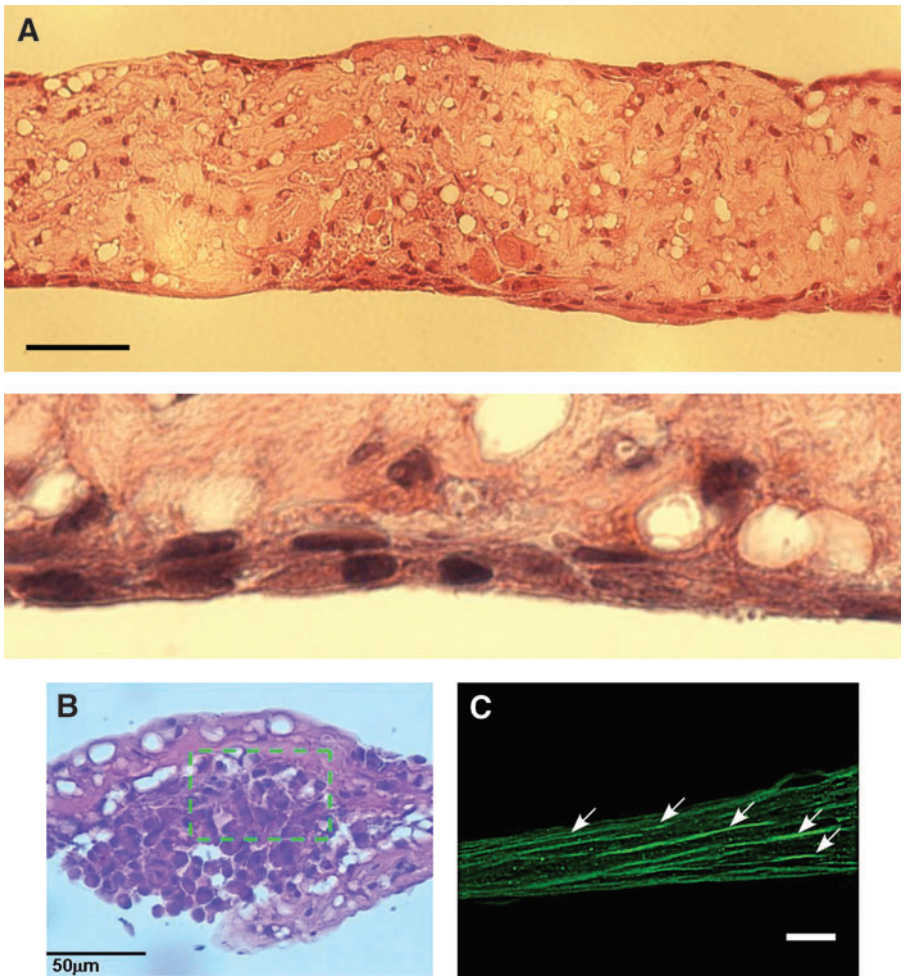

FIG. 3. Histological sections stained with hematoxylin and eosin of longitudinal sections and ×4 magnification **(A)** and lateral sections **(B)** at day14. The nuclei of the tissue-engineered skeletal muscle cells were stained purple and the cell cytoplasms were stained pink. **(C)** The longitudinal section immunofluorescent staining of tissue-engineered skeletal muscle at day 29. White arrows indicate aligned myotubes labeled for α actinin. All scale bars show 50 μm. Color images available online at www.liebertpub.com/tea

would be necessary to investigate changes of expressing some related protein, such as alpha-actinin, also MyHC, in the tissue-engineered skeletal muscle during long-term culturing. Although well-aligned myotubes could be fabricated on the gel tissue as a tissue-engineered skeletal muscle, medium circulation into the gel was necessary to develop thicker muscle tissues. Further research in neoangiogenesis[32] would promote the development of larger and thicker muscle tissues.

Cell alignment in tissue-engineered skeletal muscles

Angular deviation on five different samples was compared to evaluate the coherency of the cell alignment between a molded stretched gel and gel on a flat dish. Quantitative analysis of cell alignment revealed a strong influence from the topographic features of the mold for the muscle cells. Figure 4 reproduces representative cell culture images and relative histograms and angular deviations of the alignment angle of cells. Figure 4B shows the histogram of cellular orientation cultured in the tissue-engineered skeletal muscle. There was a peak on the longitudinal axis of the PDMS mold groove (angular mean ± SD = 2.92×10^{-1} ± 2.3°). In contrast, the histogram for cells cultured on a tissue culture dish as a control (Fig. 4D) showed a uniform distribution for the orientation angle. In comparing these angular deviations of the global alignment angle, angular deviation of the tissue-engineered skeletal muscles was significantly lower compared with the control cell culture (Fig. 4E, $p < 0.01$, $n = 5$).

The formed tissue-engineered skeletal muscles were highly aligned morphology and myotubes along the longitudinal angle of the gel structure. This myotube alignment in the gel structure would be caused by the stretching factor on the tissue-engineered skeletal muscle and form factor by the gel structure and the PDMS groove. Stretching of the myoblast culture with static stress caused parallel alignment of differentiated myotubes along the stretching direction and a longer length of the myotubes.[33] A parallel groove for the culturing substrate also caused cell orientation along the ridge of the groove texture, which had an optimum width of the groove. In our study, the PDMS mold for forming the tissue-engineered skeletal muscle with a gel mixture would affect the form factor to the muscle in the early stage of culturing. And then, the self-stretching by shrinking of the tissue-engineered skeletal muscle and that elongate shape would contribute to the alignment of the myotubes along the longitudinal direction.

Microhand powered by muscle tissue

Figure 5A shows the PDMS microhand assembled with the tissue-engineered skeletal muscle. The tissue-engineered skeletal muscle was successfully snapped on the hook of the

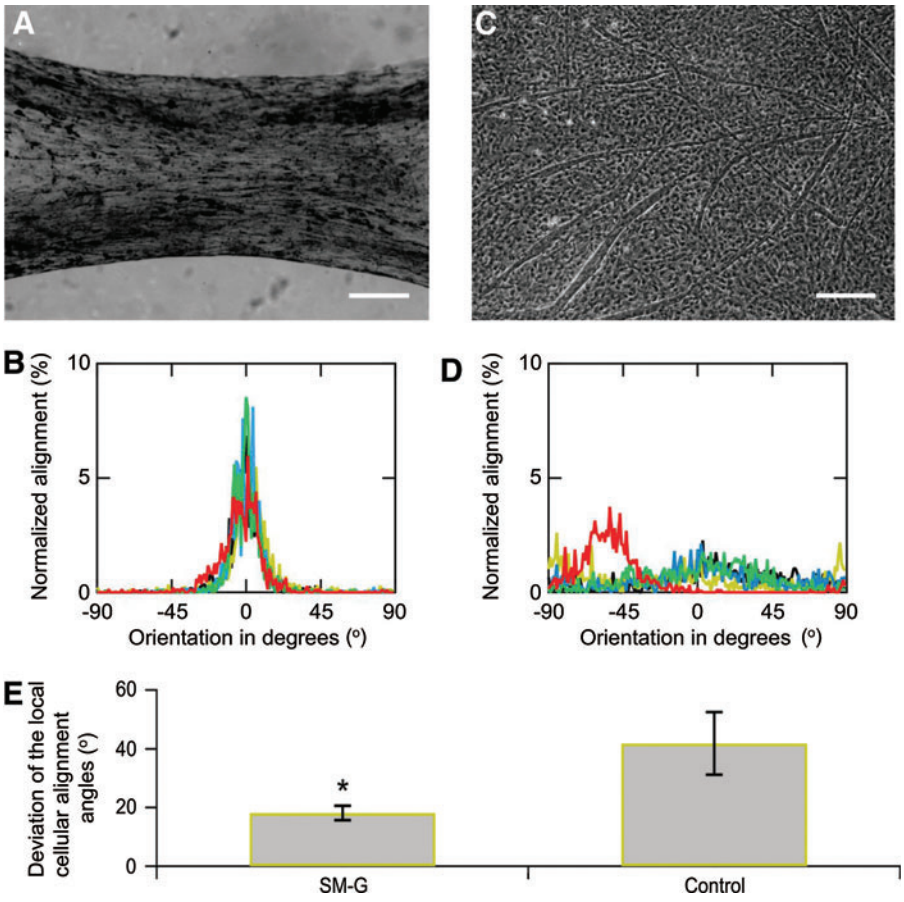

FIG. 4. Cell alignment in tissue-engineered skeletal muscles at day 12. **(A)** Phase-contrast microscope image of the tissue-engineered skeletal muscle, and **(B)** distributions of the local cellular alignment angles. **(C)** Cell culture image on a polystyrene culture dish (scale bars were 200 μm in (a) and (c)), and **(D)** corresponding distributions of the local cellular alignment angles. Cellar alignment in the tissue-engineered skeletal muscle exhibited a maximum peak as to orientation angle at the fraction of 0 degree. **(E)** Deviations of the local cellular alignment angles in tissue-engineered skeletal muscles and cell culture on dishes. Error bar was standard deviation of five independent measurements; asterisk indicates significant difference (*$p < 0.01$; t-tests; n=5). Color images available online at www.liebertpub.com/tea

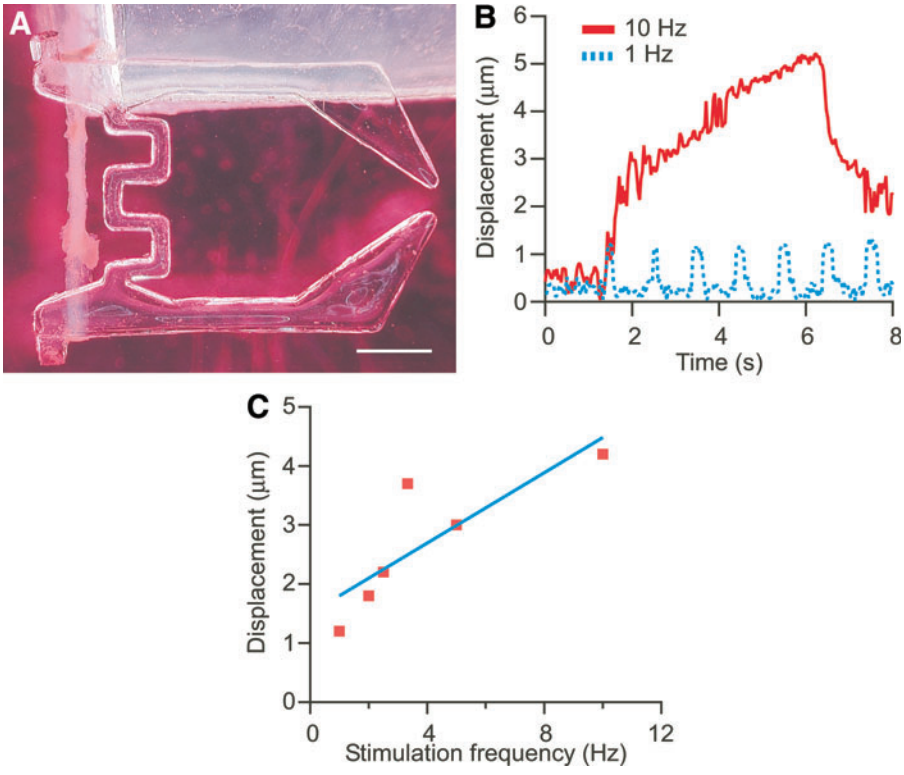

FIG. 5. A poly(dimethyl siloxane) (PDMS) gripper-type microhand with tissue-engineered skeletal muscle. **(A)** An assembly of the microhand structure and tissue-engineered skeletal muscle. The one end of the microhand was fixed to a PDMS substrate. **(B)** Displacement of the tip of the microhand responded to the frequent electrical simulation. The muscle-powered microhand was deformed by muscle contraction induced by EPS. **(C)** Relationship between displacement of the muscle-powered microhand and stimulation frequency. The scale bar shows 1 mm. Color images available online at www.liebertpub.com/tea

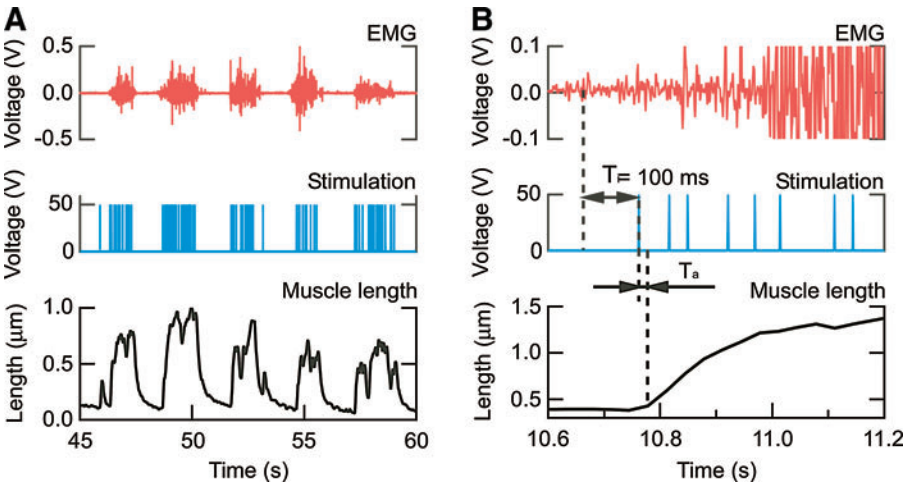

FIG. 6. Control of the gripper-type microhand by surface EMG signal. **(A)** Time course of control signals and response of the microhand to the EMG control, and **(B)** each element on a larger scale. Upper row graphs: surface EMG. Center row graphs: EPS. Lower row graphs: displacement of tissue-engineered skeletal muscle length on the microhand. T_i is the integration period for surface EMG signal to calculate the neuromimetic firing spike train. T_a is an EMD between the time of EPS onset and tissue-engineered skeletal muscle length change. EMD, electromechanical delay. Color images available online at www.liebertpub.com/tea

microhand end without damage to the tissue. At the 1-Hz pulse, the skeletal muscle contraction was synchronized with EPS. The tissue-engineered skeletal muscle could maintain a contractile state with the EPS at a 10-Hz pulse frequency. For the higher frequency of stimulation, the contraction was changed from twitching to tetanic contraction (Fig. 5B and Supplementary movie). The driving force was calculated from the tip displacement of the microhand when the skeletal muscle was stimulated. The frequency response of the peak maximum force due to the muscle contraction is shown in Figure 5C. The contraction force of the tissue-engineered skeletal muscle increased with increasing frequency of the electrical stimulation. The contraction force of natural skeletal muscles is generally controlled by varying the frequency of action potentials and motor unit recruitment.[34] Thus, the skeletal muscle tissue, fabricated with our protocol, had a similar tetanic contraction property compared to the natural skeletal muscle and would be able to control the dynamic motion of prosthesis.

Motion control of the muscle-powered microhand with EMG signals

The microhand was opened by the neuromimetic firing spike train processed from the surface EMG signal. The movement of the microhand was related to the envelope of the surface EMG signals (Fig. 6A). This result suggested that the assembly of the tissue fabricated from the living muscle and the PDMS structure could be controlled by the surface EMG signal through the neuromimetic firing spike train. Figure 6B shows an electromechanical delay (EMD) of 30 ms ($=T_a$) of the tissue-engineered skeletal muscle on the microhand movement when responding to the neuromimetic firing spike train. Thus, total EMD of the tissue-engineered skeletal muscle was 130 ms, which was totaled T_a and the $T_i = 100$ ms of the integration period for surface EMG signal to calculate the neuromimetic firing spike train. In the human body, EMD is caused between neural stimulation of a muscle and generation of the muscle tension.[35] This native EMD was reported as 50 ms in previous research.[36] This fact indicated that the neuromuscular control could compensate the EMD to gain stability of the delayed system. Surface EMG was also leading a joint torque about 40–90 ms from the beginning of the surface EMG signal.[37] Therefore, the equivalent EMD of the tissue-engineered skeletal muscle to the native EMD would contribute similar dynamics to the native muscle control.

Conclusion

This article described surface EMG controlled of a prosthesis powered by a tissue-engineered skeletal muscle (a living prosthesis) with a final goal of practical application. To demonstrate a prototype of the living prosthesis, we fabricated the skeletal muscle tissue, which had highly aligned cells and similar contraction properties to a natural skeletal muscle. The prototype living prosthesis consisting of a PDMS microhand and a tissue-engineered skeletal muscle was controlled by the neuromimetic spike train from the surface EMG signal. In the future, living prostheses will be able to produce active forces using energy in the human body and development will move toward complete reconstruction of functionality of lost limbs.

Acknowledgments

This work was partly supported by Grants-in-Aid for Scientific Research from the Ministry of Education, Culture, Sports, Science and Technology (Biomanipulation) in Japan No. 18656042 and No. 20034017, and Industrial Technology Research Grant Program in 2007 from New Energy and Industrial technology Development Organization (NEDO) of Japan.

Disclosure Statement

No competing financial interests exist.

References

1. Wessberg, J., Stambaugh, C.R., Kralik, J.D., Beck, P.D., Laubach, M., Chapin, J.K., Kim, J., Biggs, S.J., Srinivasan, M.A., and Nicolelis, M.A.L. Real-time prediction of hand

trajectory by ensembles of cortical neurons in primates. Nature **408,** 361, 2000.
2. Koike, Y., and Kawato, M. Estimation of dynamic joint torques and trajectory formation from surface electromyography signals using a neural network model. Biol Cybern **73,** 291, 1995.
3. Choi, K., Hirose, H., Sakurai, Y., Iijima, T., and Koike, Y. Prediction of arm trajectory from the neural activities of the primary motor cortex with modular connectionist architecture. Neural Netw **22,** 1214, 2009.
4. Yokoi, H., Arieta, A.H., Katoh, R., Yu, W., Watanabe, I., and Maruishi, M. Mutual adaptation in a prosthetics application. In: Iida, F., Pfeifer, R., Steels, L., and Kuniyoshi, Y., eds. *Embodied Artificial Intelligence.* Berlin, Heidelberg: Springer Berlin Heidelberg, 2004, vol. 3139, pp. 146–159.
5. Okuno, R., Akazawa, K., and Yoshida, M. Biomimetic myoelectric hand with voluntary control of finger angle and compliance. Front Med Biol Eng **9,** 199, 1999.
6. Miller, L.A., Stubblefield, K.A., Lipschutz, R.D., Lock, B.A., and Kuiken, T.A. Improved myoelectric prosthesis control using targeted reinnervation surgery: a case series. IEEE Trans Neural Syst Rehabil Eng **16,** 46, 2008.
7. Vandenburgh, H.H., Karlisch, P., and Farr, L. Maintenance of highly contractile tissue-cultured avian skeletal myotubes in collagen gel. In Vitro Cell Dev Biol **24,** 166, 1988.
8. Okano, T., and Matsuda, T. Tissue engineered skeletal muscle: preparation of highly dense, highly oriented hybrid muscular tissues. Cell Transplant **7,** 71, 1998.
9. Breuls, R.G.M., Mol, A., Petterson, R., Oomens, C.W.J., Baaijens, F.P.T., and Bouten, C.V.C. Monitoring local cell viability in engineered tissues: a fast, quantitative, and nondestructive approach. Tissue Eng **9,** 269, 2003.
10. Vandenburgh, H.H., Swasdison, S., and Karlisch, P. Computer-aided mechanogenesis of skeletal muscle organs from single cells *in vitro*. FASEB J **5,** 2860, 1991.
11. Dennis, R.G., and Kosnik, P.E., 2nd. Excitability and isometric contractile properties of mammalian skeletal muscle constructs engineered *in vitro*. In Vitro Cell Dev Biol Anim **36,** 327, 2000.
12. Dennis, R.G., Kosnik, P.E., 2nd, Gilbert, M.E., and Faulkner, J.A. Excitability and contractility of skeletal muscle engineered from primary cultures and cell lines. Am J Physiol Cell Physiol **280,** C288, 2001.
13. Y.-C. Huang, Dennis, R.G., Larkin, L., and Baar, K. Rapid formation of functional muscle *in vitro* using fibrin gels. J Appl Physiol **98,** 706, 2005.
14. Lam, M.T., Y.-C. Huang, Birla, R.K., and Takayama, S. Microfeature guided skeletal muscle tissue engineering for highly organized 3-dimensional free-standing constructs. Biomaterials **30,** 1150, 2009.
15. Bach, A.D., Beier, J.P., Stern-Staeter, J., and Horch, R.E. Skeletal muscle tissue engineering. J Cell Mol Med **8,** 413, 2004.
16. Hinds, S., Bian, W., Dennis, R.G., and Bursac, N. The role of extracellular matrix composition in structure and function of bioengineered skeletal muscle. Biomaterials **32,** 3575, 2011.
17. Powell, C.A., Smiley, B.L., Mills, J., and Vandenburgh, H.H. Mechanical stimulation improves tissue-engineered human skeletal muscle. Am J Physiol Cell Physiol **283,** C1557, 2002.
18. Bian, W., and Bursac, N. Engineered skeletal muscle tissue networks with controllable architecture. Biomaterials **30,** 1401, 2009.
19. Neumann, T., Hauschka, S.D., and Sanders, J.E. Tissue engineering of skeletal muscle using polymer fiber arrays. Tissue Eng **9,** 995, 2003.
20. Eschenhagen, T., Fink, C., Remmers, U., Scholz, H., Wattchow, J., Weil, J., Zimmermann, W., Dohmen, H.H., Schäfer, H., Bishopric, N., Wakatsuki, T., and Elson, E.L. Three-dimensional reconstitution of embryonic cardiomyocytes in a collagen matrix: a new heart muscle model system. FASEB J **11,** 683, 1997.
21. W.-H. Zimmermann, Melnychenko, I., Wasmeier, G., Didié, M., Naito, H., Nixdorff, U., Hess, A., Budinsky, L., Brune, K., Michaelis, B., Dhein, S., Schwoerer, A., Ehmke, H., and Eschenhagen, T. Engineered heart tissue grafts improve systolic and diastolic function in infarcted rat hearts. Nat Med **12,** 452, 2006.
22. Kosnik, P.E., Faulkner, J.A., and Dennis, R.G. Functional development of engineered skeletal muscle from adult and neonatal rats. Tissue Eng **7,** 573, 2001.
23. Horiguchi, H., Imagawa, K., Hoshino, T., Akiyama, Y., and Morishima, K. Fabrication and evaluation of reconstructed cardiac tissue and its application to bio-actuated microdevices. IEEE Trans Nanobiosci **8,** 349, 2009.
24. Lam, M.T., Sim, S., Zhu, X., and Takayama, S. The effect of continuous wavy micropatterns on silicone substrates on the alignment of skeletal muscle myoblasts and myotubes. Biomaterials **27,** 4340, 2006.
25. Hosseini, V., Ahadian, S., Ostrovidov, S., Camci-Unal, G., Chen, S., Kaji, H., Ramalingam, M., and Khademhosseini, A. Engineered contractile skeletal muscle tissue on a microgrooved methacrylated gelatin substrate. Tissue Eng Part A **18,** 2453, 2012.
26. Dhawan, V., Lytle, I.F., Dow, D.E., Y.-C. Huang, and Brown, D.L. Neurotization improves contractile forces of tissue-engineered skeletal muscle. Tissue Eng **13,** 2813, 2007.
27. Akiyama, Y., Terada, R., Hashimoto, M., Hoshino, T., Furukawa, Y., and Morishima, K. Rod-shaped tissue engineered skeletal muscle with artificial anchors to utilize as a bioactuator. J Biomech Sci Eng **5,** 236, 2010.
28. Hsohino, T., and Morishima, K. Muscle-powered cantilever for microtweezers with an artificial micro skeleton and rat primary myotubes. J Biomech Sci Eng **5,** 245, 2010.
29. Ahadian, S., Ramón-Azcón, J., Ostrovidov, S., Camci-Unal, G., Hosseini, V., Kaji, H., Ino, K., Shiku, H., Khademhosseini, A., and Matsue, T. Interdigitated array of Pt electrodes for electrical stimulation and engineering of aligned muscle tissue. Lab Chip **12,** 3491, 2012.
30. Rezakhaniha, R., Agianniotis, A., Schrauwen, J.T.C., Griffa, A., Sage, D., Bouten, C.V.C., van de Vosse, F.N., Unser, M., and Stergiopulos, N. Experimental investigation of collagen waviness and orientation in the arterial adventitia using confocal laser scanning microscopy. Biomech Model Mechanobiol **11,** 461, 2012.
31. Fujita, H., Shimizu, K., and Nagamori, E. Novel method for fabrication of skeletal muscle construct from the C2C12 myoblast cell line using serum-free medium AIM-V. Biotechnol Bioeng **103,** 1034, 2009.
32. Koga, Y., Komuro, Y., Yamato, M., Sueyoshi, N., Kojima, Y., Okano, T., and Yanai, A. Recovery course of full-thickness skin defects with exposed bone: an evaluation by a quantitative examination of new blood vessels. J Surg Res **137,** 30, 2007.
33. Vandenburgh, H.H., and Karlisch, P. Longitudinal growth of skeletal myotubes *in vitro* in a new horizontal mechanical cell stimulator. In Vitro Cell Dev Biol **25,** 607, 1989.

34. Close, R. Dynamic properties of fast and slow skeletal muscles of the rat after nerve cross-union. J Physiol (Lond) **204,** 331, 1969.
35. Valero-Cuevas, F.J., Zajac, F.E., and Burgar, C.G. Large index-fingertip forces are produced by subject-independent patterns of muscle excitation. J Biomech **31,** 693, 1998.
36. Cavanagh, P., and Komi, P. Electromechanical delay in human skeletal muscle under concentric and eccentric contractions. Eur J Appl Physiol Occup Physiology **42,** 159, 1979.
37. Li, L., and Baum, B.S. Electromechanical delay estimated by using electromyography during cycling at different pedaling frequencies. J Electromyogr Kinesiol **14,** 647, 2004.

Address correspondence to:
Keisuke Morishima, PhD
Department of Mechanical Engineering
Osaka University
2-1 Yamadaoka
Suita
Osaka 565-0871
Japan

Received: July 10, 2012
Accepted: February 20, 2013
Online Publication Date: June 6, 2013